Transient diffusion and two-regime localization of discrete breatherlike excitations in nonlinear Schrödinger lattice with disorder

Zhi-Yuan Sun[1,2,*] and Xin Yu[1,†]

[1]*Institute of Fluid Mechanics, Beihang University, Beijing 100191, China*

[2]*International Research Institute for Multidisciplinary Science, Beihang University, Beijing 100191, China*

(Received 20 February 2019; published 2 August 2019)

We systematically simulate and analyze the motion of discrete breatherlike excitations (DBEs) in the nonlinear Schrödinger lattice with random potentials. A universal transient diffusion of the DBEs is observed for short timescales ($t \lesssim 10^3$). For longer timescales (t up to 10^5), the DBEs become localized. Such localization, depending on the DBE powers, has two different regimes: Regime I is the Anderson-like localization induced by the disorder, while Regime II is an enhanced localization attributed to both the disorder and discreteness. Our study is expected to shed light on understanding the interplay between disorder and strong nonlinearity, from the diffusive transport and localization properties of nonlinear localized excitations in random media.

DOI: 10.1103/PhysRevE.100.022202

I. INTRODUCTION

The interplay between disorder and nonlinearity is an important subject extensively studied in different physical systems. One open question is how the famous Anderson localization (AL) in random media [1] is influenced by the presence of nonlinearity [2,3]. This question has been theoretically discussed within the framework of the nonlinear Schrödinger (NLS) lattices [4–6]. Numerical simulations demonstrated the AL would be broken up by a weak cubic nonlinearity, leading to a subdiffusive spreading of the wave packets [7,8]. Meanwhile, Fishman *et al.* [4] used a perturbation approach to point out that such a problem remained inclusive for long-time evolution. The experiments on optics [9,10] and cold atoms [11,12] provided evidence of the wave-packet localization, with the combined effects of disorder and nonlinearity. A recent observation of granular chain [13] showed the destruction of the AL, as well as the occurrence of a superdiffusive energy transport. Generally speaking, these studies present fruitful results but are mainly focused, on one hand, on the spreading of wave packets—the "wave nature" of lattice excitations.

On the other hand, existence of the long-lived discrete breathers, the spatially localized and time-periodic stable excitations, is a remarkable manifestation of nonlinearity, that appear, e.g., in nonlinear optics and Bose-Einstein condensates (BECs) [14–21]. Such intrinsic localized structures, embodying more "particlelike features," transport mass and energy when they are mobile in a lattice. In this work, we consider the discrete breatherlike excitations (DBEs), whose localized density oscillates with time (they may not be strictly periodic and be named breathing solitons elsewhere). The collision of DBEs with ordered impurities can be seen in Refs. [22,23]. However, to our knowledge, the motion of DBEs in a disordered lattice, as an aspect of the interaction between disorder and strong nonlinearity, has been insufficiently studied, which will be the subject here. It has to be mentioned that some pioneering works considered the transport of solitary waves in certain continuous systems with disorder; for example, see the celebrated Gordon-Haus effect [24] and its nonlocal counterpart [25,26]. The Brownian soliton motion (normal diffusion) [27,28] and the so-called AL of solitons [29–31] were reported as well. Nevertheless, our results for the discrete system will be quite different, with a transient diffusion and two regimes of localization revealed for the DBEs.

II. MODEL AND METHOD

For the above purpose, we consider the following one-dimensional (1D) time-dependent NLS lattice:

$$i\frac{\partial \psi_n}{\partial t} = -(\psi_{n-1} + \psi_{n+1}) - \nu|\psi_n|^2\psi_n + \epsilon_n\psi_n\,, \qquad (1)$$

where ψ_n is the dimensionless wave function at site n and time t, while ν characterizes the strength of the cubic nonlinearity. The random potential ϵ_n satisfies the normal distribution with zero mean value and standard deviation σ, that is, $\langle\epsilon_n\rangle = 0$ and $\langle\epsilon_n\epsilon_{n'}\rangle = \sigma^2\delta(n-n')$, where the angular brackets stand for statistical averaging. Equation (1) can be a prototype lattice model describing the propagation of optical and atomic wave packets in a disordered environment [4,9,10,17].

Without random potentials ($\epsilon_n \equiv 0$), one effective way to generate the long-lived DBEs, with their lifetimes $t \gtrsim 10^5$, is starting from an initially localized wave packet, e.g., those with the Gaussian or hyperbolic shape [17,20]. The profiles of these DBEs are asymptotically well fitted, in the form $\sinh(\mu_1)/\cosh(\mu_2 n)$, where μ_1 and μ_2 are close to each other [17]. Therefore we will practically use the initial state $\psi_n(t=0) = \sinh(\mu)/\cosh(\mu n)$ to produce the DBEs in the disordered lattice ($\epsilon_n \neq 0$), with μ viewed as the parameter relating to the power of DBE [32]. This initial condition, with the parameters in our context, locates in the non-Gibbs phase

*sunzhiyuan137@aliyun.com

†yuxin@buaa.edu.cn

of the NLS lattice, where the formation of long-lasting DBEs was reported [33,34]. Hereby we stress that the relatively strong nonlinearity, compared with the strength of disorder, is addressed in our work, keeping the DBEs neither breaking up nor radiating quickly, so that they can evolve for a considerable long time.

To investigate the particlelike motion of DBEs, we concentrate on random walks of these localized excitations, considering the basic quantity: the ensemble-averaged mean squared displacement (eMSD) $\langle x^2(t)\rangle$, defined as $\langle x^2(t)\rangle \triangleq \frac{1}{N}\sum_{i=1}^{N} x_i^2(t)$, where $x(t)$ is the center of mass of the DBE for the density $|\psi_n(t)|^2$. For a classical particle, the eMSD can characterize either a Brownian motion $\langle x^2(t)\rangle \sim t$ or an anomalous diffusion $\langle x^2(t)\rangle \sim t^\gamma$ with $\gamma \neq 1$ for a certain timescale. Anomalous diffusion plays an important role in complex systems and has been discussed using a statistical framework in different contents [35]. It typically includes subdiffusion ($0 < \gamma < 1$), superdiffusion ($1 < \gamma < 2$), and even a less understood case, hyperdiffusion ($\gamma > 2$). These anomalous diffusions appear in various occasions: Subdiffusion has been observed in the stochastic motion of mRNA molecules [36] and also in the particle tracking of polystyrene beads in micellar solutions [37]. Superdiffusion has been reported for the transport of polymeric particles in living cells [38] and for the diffusion of ellipsoids in bacterial suspensions [39], as well as for the light in the engineered optical materials [40]. Also, a transition from the short-time subdiffusion to the longer-time normal diffusion was shown for telomeres in the nucleus of mammalian cells [41]. In this study, we find a transient diffusion of DBEs for a short timescale, induced by disorder, containing time intervals with the different scaling exponents γ, which to our best knowledge has never been reported before.

We performed extensive simulations to analyze the DBE motion. Equation (1) was integrated by using a fourth-order Runge-Kutta scheme with the periodic boundary conditions. The size of the lattice with $n \in [-L, L]$ was chosen large enough ($L = 300$) so the DBEs are far away from the boundaries. The step size of time discretization was $\Delta t = 0.01$, and the total computational time was up to $T = 10^5$. Our statistical results below were derived by averaging over $N = 256$ realizations, while in each realization, the DBE was checked not to break up and remained localized at all times [42].

III. RESULTS AND DISCUSSIONS

Figure 1(a) displays a typical motion of the DBE in a random potential, while nine different realizations of motion trajectories are shown in Fig. 1(b). The initial state, after a very short time [$\sim$10 time units (TUs)], evolves into a DBE, scattered by the random impurities to experience transverse displacements larger than the scale of the DBE for many realizations. Hence, the diffusive behavior can exist in analog with that for classical particles. The DBE may change its moving direction at certain spots of "strong" impurities and oscillate for many times before it gradually becomes localized for the long timescale. Apparently, these diffusion and localization are strongly nonlinear phenomena, since the DBEs are robust enough to keep their identities during the motions [45].

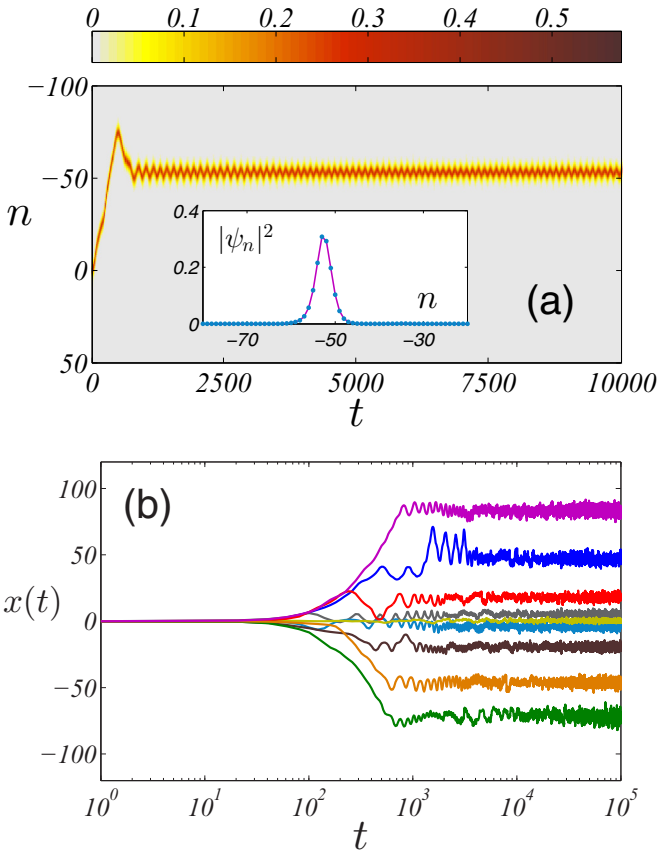

FIG. 1. (a) Density demonstration $|\psi_n(t)|^2$ of the DBE in the lattice for a realization of random potential, with the embedded panel showing the profile at $t = 10^5$. (b) Motion trajectories for the center of mass of the DBEs for nine independent realizations of the random potentials. For both subfigures, the parameters are $\mu = 0.7$, $\sigma = 0.01$, and $\nu = 1$.

In Fig. 2(a) we plot the eMSD $\langle x^2(t)\rangle$ as a function of the time t on a log-log scale for five orders of magnitude, with the same representative parameters shown in Fig. 1. As observed, diffusion of the DBEs persists at short timescales ($t \lesssim 10^3$), and the eMSD reaches a plateau (the localization of DBEs) at the longer time range. Analysis of the data (see Table I below) suggests that the diffusive process may consist of three different intervals: a diffusion of $\sim$40 TUs with $\gamma \approx 3.2$, a diffusion of $\sim$200 TUs with $\gamma \approx 1.6$, and a diffusion of $\sim$100 TUs with $\gamma \approx 0.8$. In fact, the length of these diffusion intervals would increase remarkably as for a weaker randomness, but with the main features unchanged.

To further study the diffusive process ($t \lesssim 10^3$), the time-averaged MSD (tMSD) of an individual trajectory is introduced as $\overline{\delta^2(\Delta, T)} = \frac{1}{T-\Delta}\int_0^{T-\Delta}[x(t+\Delta) - x(t)]^2\, dt$ [35], where the so-called lag time $\Delta \ll T$ defines a time window slid along the time series $x(t)$ (here we use $0 < \Delta \leqslant T/10$). For an ergodic system, the equivalence $\langle x^2(\Delta)\rangle = \lim_{T\to\infty} \overline{\delta^2(\Delta, T)}$ is necessarily expected with the identification $t \leftrightarrow \Delta$, and the opposite for a nonergodic system [35,46–48]. Mithun *et al.* have recently found a weak nonergodic phase of the NLS lattice dynamics [49].

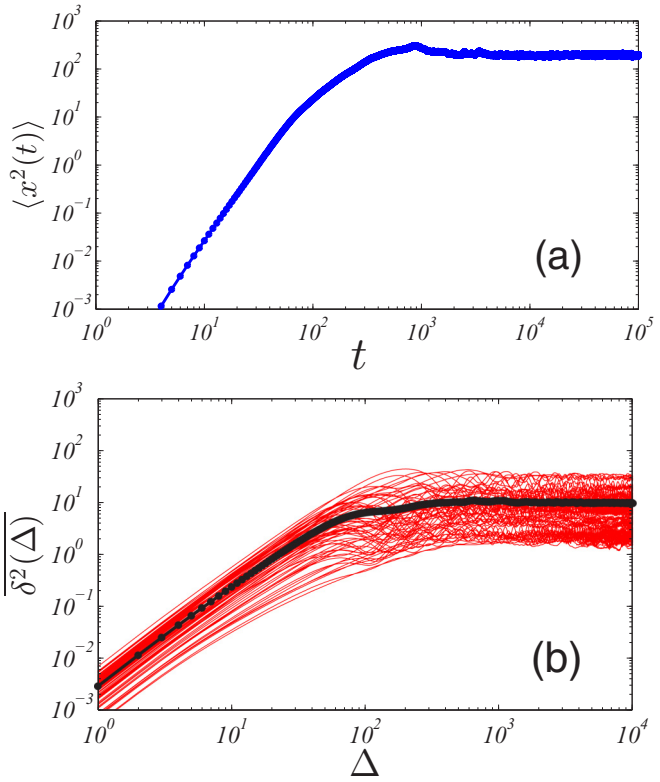

FIG. 2. (a) The eMSD $\langle x^2(t)\rangle$ as a function of the time t. (b) The tMSDs $\overline{\delta^2(\Delta)}$ ($T = 10^5$) for individual trajectories as functions of the lag time Δ, and the black bold curve denotes the trajectory-averaged tMSD $\langle\overline{\delta^2(\Delta)}\rangle$. All these quantities are evaluated from $N = 256$ independent realizations. The parameters are $\mu = 0.7$, $\sigma = 0.01$, and $\nu = 1$.

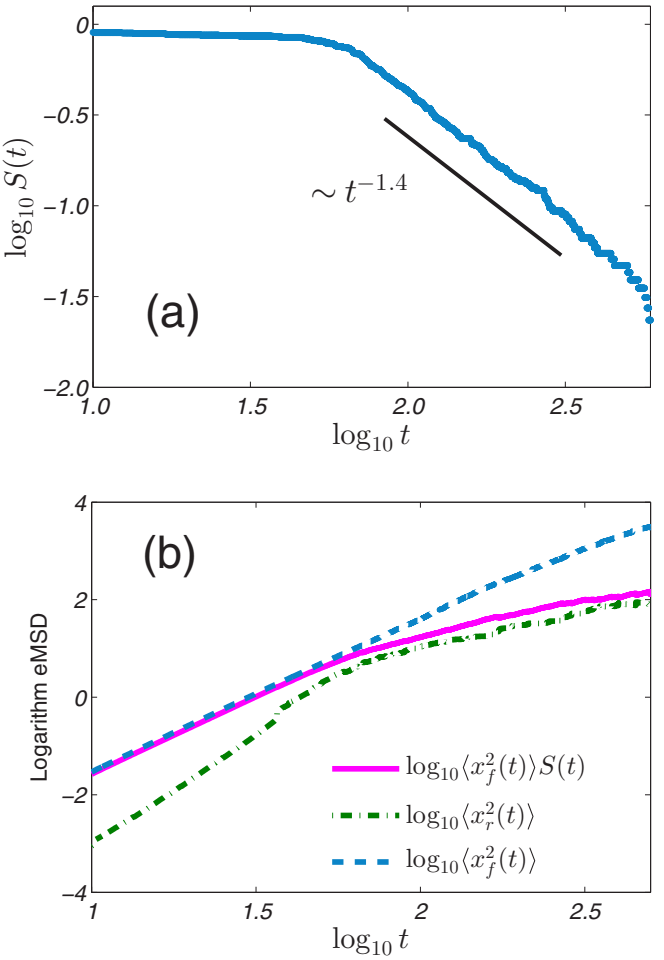

FIG. 3. (a) $S(t)$ as a function of the time t (logarithm plots). (b) Comparison of $\langle x_f^2(t)\rangle$, $\langle x_f^2(t)\rangle S(t)$, and $\langle x_r^2(t)\rangle$, in which we see the suppressing effect of $S(t)$ on $\langle x_f^2(t)\rangle$. The parameters are $\mu = 0.70$, $\sigma = 0.01$, $\nu = 1$, and $N = 256$.

Figure 2(b) shows the tMSDs $\overline{\delta^2(\Delta)}$ up to $\Delta = 10^4$, which also cover the intervals of short-time diffusion, as well as a longer-time localization, but the result obviously varies from one individual trajectory to another. We consider the trajectory-averaged tMSD $\langle\overline{\delta^2(\Delta)}\rangle$ for finite T [35,47,48] and discover the inequality $\langle x^2(\Delta)\rangle \neq \langle\overline{\delta^2(\Delta)}\rangle$ for the diffusion process. Such disparity between the eMSD and the trajectory-averaged tMSD ($t \lesssim 10^3$) appears to be kept as T grows (see Appendix A). These facts may indicate that the time averages are different from the ensemble averages within our computational limit. Systematic simulations have confirmed, for a range of initial parameters ($\mu = 0.5$–0.9), the DBEs indeed undergo transient diffusion before their localization (see Appendix B).

To better understand the transient behavior of the diffusive process, we divide the DBEs into two classes at the time t: One is the "free" DBE that propagates unidirectionally in the interval $[0, t]$ (without change of the sign of its velocity); the other one is the DBE that alters its velocity sign at least once in this interval. The eMSD for these two classes of DBEs are denoted as $\langle x_f^2(t)\rangle$ and $\langle x_r^2(t)\rangle$, respectively. Data analysis shows $\langle x_f^2(t)\rangle \gg \langle x_r^2(t)\rangle$ for most of the diffusive regions, and we can derive $\langle x^2(t)\rangle \approx \langle x_f^2(t)\rangle S(t) + \langle x_r^2(t)\rangle$ with $S(t) = N_f(t)/N$, where $N_f(t)$ is the time-dependent number of the free DBEs (see Appendix C). Take the case of $\mu = 0.70$ as an example. For the initial stage, when the number of the free DBEs is dominated, we have $S(t) \approx 1$, so that $\langle x^2(t)\rangle \approx \langle x_f^2(t)\rangle \sim t^{3.2}$. During the intermediate stage, $S(t)$ is found to decrease with time, in the form of $S(t) \sim t^{-1.4}$ [see Fig. 3(a)], which suppresses $\langle x_f^2(t)\rangle$ and makes both superdiffusive terms $\langle x_f^2(t)\rangle S(t)$ and $\langle x_r^2(t)\rangle$ comparable [see Fig. 3(b)], finally resulting in their addition, i.e., $\langle x^2(t)\rangle$, to be superdiffusive as well. For the last stage before the plateau, $S(t)$ becomes considerably small, and the major contribution to the spreading is due to the second class of DBEs, which are sufficiently constrained by the disorder, such that an interval of diffusion with $\gamma < 1$ occurs before the localization. By checking the data of $\mu = 0.50 \sim 0.90$, we further confirmed such a mechanism to be generally effective for interpreting the transient diffusive behaviors studied in this work.

Now we discuss the localization with detailed information. According to Fig. 2(a), we first define the following quantity to characterize the plateau as

$$L \triangleq \frac{1}{T}\int_0^T \langle x^2(t)\rangle\, dt\,, \tag{2}$$

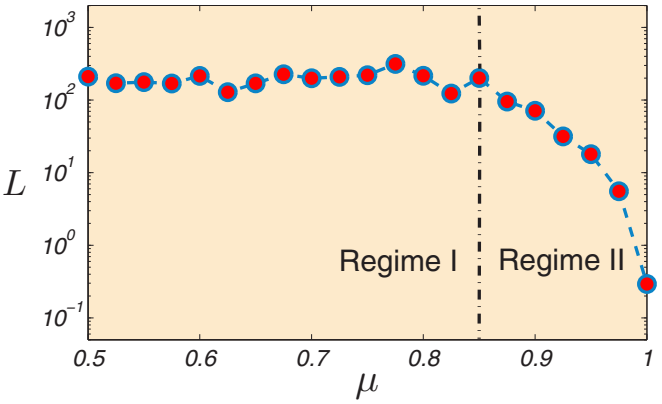

FIG. 4. Dependence plots of L on μ. Each plotted value is evaluated from $N = 256$ independent realizations. The parameters are $\sigma = 0.01$ and $\nu = 1$.

with $T = 10^5$. The formulas (2) can be used to describe the length of the localization: a larger L means a wider distribution of the localized DBEs, while oppositely, a smaller L indicates that the DBEs are confined in a narrower spatial region. The dependence of L on the parameter μ is obtained from systematic simulations of the DBE motions, as shown in Fig. 4. We clearly see that, with an increase of the DBE powers, there exist two regimes with different tendencies. In Regime I, L is almost independent of μ, while L quickly decreases by about two orders of magnitude in Regime II. The transition from Regime I to Regime II occurs near $\mu = 0.85$.

Such a transition hereby can be understood, by using a *disordered version* of the Peierls-Nabarro (PN) potential [50]. This effective potential, approximately describing the DBE motion, is made up of two parts: One is the discreteness-generated potential $\mathcal{U}_d \sim -\frac{2\pi^2\nu\sinh^2(\mu)}{\mu^3\sinh(\pi^2/\mu)}\cos(2\pi x)$, and the other one is the randomness-generated potential $\mathcal{U}_r$, with $\langle\mathcal{U}_r^2\rangle \sim \sigma^2\lambda^2(\mu)$, where $\lambda(\mu)$ is a μ-dependent function [one can see its numerical form in Fig. 1(c) of Ref. [50]]. The interaction between these two potentials is estimated by the following ratio:

$$\kappa(\mu, \sigma/\nu) = \frac{\sigma}{\nu}\left[\frac{\mu^3\sinh(\pi^2/\mu)\lambda(\mu)}{2\pi^2\sinh^2(\mu)}\right], \tag{3}$$

in which, besides the strength of disorder and nonlinearity, the parameter μ also plays an important role. For the case of Fig. 4, the variation of κ with μ is illustrated in Appendix D. We find $\kappa > 10^1$ in Regime I, meaning that $\mathcal{U}_r$ is at least one order of magnitude stronger than $\mathcal{U}_d$, so the localization in this regime should be dominated by the effect of disorder. In Regime II, the strength of $\mathcal{U}_r$ and $\mathcal{U}_d$ reach the same order of magnitude, such that this is a regime where the localization is resulted from the mutual interplay of both the disorder and discreteness. With μ increasing, the localization of Regime II is apparently enhanced, since the potential barrier of $\mathcal{U}_d$ becomes larger for the DBE with higher power. Formula (3) can be effective in qualitatively analyzing the localization of DBEs for different ratios of σ/ν: For stronger disorder, we observe that the transition point from Regime I to Regime II moves to a larger value of μ, which is reasonable because of the upper shift of the $\kappa(\mu)$ curve (see Appendix D).

Are these transient diffusive and localization behaviors universal for other types of disorder? At least we have checked the DBE motions in the uniformly distributed random potential, i.e., $\epsilon_n \in \text{unif}[-W, +W]$, and have found the results present general similarity with the above discussions (see Appendix E).

IV. OUTLOOKS AND SUMMARY

So what further can we benefit from this study? First of all, these systematic behaviors are due to the interaction of disorder and strong nonlinearity, which reveal the novel scopes of the particlelike motion of the DBEs, rather than the diffusive spreading of wave packets induced by weak nonlinearity. One notices that for strong nonlinearity, a single-site excitation cannot uniformly spread over the entire disordered lattice, leaving partially the wave packet staying localized. This self-trapping was rigorously proved and related to the presence of time-quasiperiodic breatherlike states [51,52]. Here we might expect the location of such trapped states, depending on their power, to fulfill either regime of the transient localization for long-time measurement. Second, as the DBE's power, linked with its shape structure, is a factor that influences the properties of the DBE diffusion and localization, one may experimentally engineer the DBEs in optical lattices of waveguide arrays (or BEC setup), to realize their controllable transport to some extent. Finally, whether we can make some judgment on ergodicity from longer-time ($t > 10^5$) simulation of the DBE transport seems to be an open question.

In summary, we have observed transient diffusion and two-regime localization of DBEs by systematically simulating a prototype NLS lattice with random potentials. The diffusion shows an inequivalence of the eMSD and the tMSD for the DBE's center of mass within our computational limit. The transition, from an Anderson-like localization to an enhanced localization, is qualitatively explained by the PN potential with disorder. These phenomena appear to present a high similarity for different types of randomness.

ACKNOWLEDGMENTS

Z.-Y.S. thanks S. Fishman and A. Soffer for initializing this project during his postdoc research in Technion. The referees are appreciated for their valuable and stimulating comments. This work is supported by the Zhuoyue Talent Program of Beihang University and by the Fundamental Research Funds for the Central Universities.

APPENDIX A: $\langle\overline{\delta^2(\Delta)}\rangle/\langle x^2(\Delta)\rangle$ FOR FINITE T

To describe the disparity between the tMSD and the eMSD, we use the parameter $\mathcal{EB}(\Delta) \triangleq \langle\overline{\delta^2(\Delta)}\rangle/\langle x^2(\Delta)\rangle$ as the ratio of these two averages. Shown in Fig. 5, the dependence of the $\mathcal{EB}(\Delta)$ curve on T is small, and the function almost converges as T grows and approaches 10^5. Hence the tMSD is generally unequal to the eMSD for the short-time diffusion process, and there is no indication that the equality might hold within our computational limit.

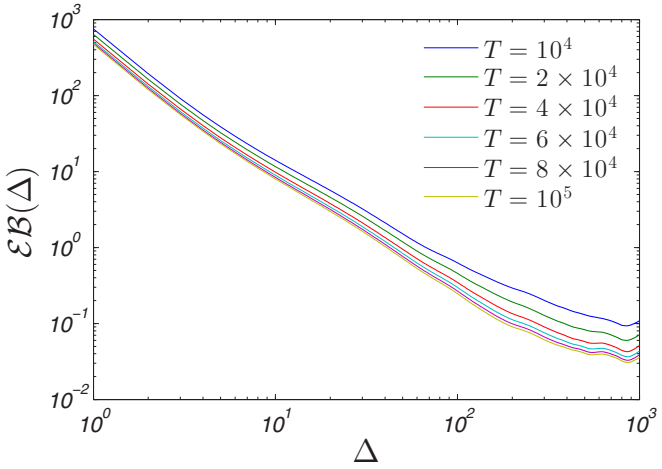

FIG. 5. The parameter $\mathcal{EB}(\Delta)$ as a function of Δ for T varying from 10^4 to 10^5 (the curves from top to bottom correspond to $T = 10^4$ to $T = 10^5$). The parameters are $\mu = 0.7$, $\sigma = 0.01$, $\nu = 1$, and $N = 256$.

APPENDIX B: SIMULATION RESULTS FOR $\mu = 0.50$–0.90

We have performed a series of simulations, while μ varies from 0.50 to 0.90 with a step size of 0.025. Generally speaking, the higher-power DBE, with larger value of μ, has a larger amplitude and a narrower width, which presents a better stability against the perturbation on its profile. However, we carefully checked each realization, to make sure that, with our parameters, both of the low- and high-power DBEs keep compact and localized during their transport (no less than $t = 10^5$). Typical results are shown in Fig. 6, and relevant data analysis can be seen in Table I.

TABLE I. Diffusive properties of the DBE dynamics for $\mu = 0.50$, 0.60, 0.70, and 0.80. The eMSD and tMSD curves are fitting to $\langle x^2(t)\rangle \sim t^{\gamma}$ and $\langle\overline{\delta^2(\Delta)}\rangle \sim \Delta^{\gamma'}$ for different time intervals. The $R^2 > 0.99$ is kept for each fit unless otherwise stated.

Time interval	γ	γ'
	$\mu = 0.50$	
10–80	2.92 ± 0.01	1.60 ± 0.01
120–350	1.86 ± 0.01	0.59 ± 0.01
440–560	0.97 ± 0.01	0.26 ± 0.01
	$\mu = 0.60$	
10–60	3.02 ± 0.01	1.63 ± 0.01
100–350	1.67 ± 0.01	0.47 ± 0.01
400–500	0.90 ± 0.01	0.19 ± 0.01
	$\mu = 0.70$	
10–50	3.17 ± 0.01	1.67 ± 0.01
80–320	1.62 ± 0.01	0.37 ± 0.01[a]
350–480	0.84 ± 0.01	0.13 ± 0.01[b]
	$\mu = 0.80$	
10–50	3.31 ± 0.01	1.59 ± 0.02
80–380	1.41 ± 0.01	Nearly localized
410–520	0.73 ± 0.01	Nearly localized

[a] $R^2 = 0.983$ for this fit.
[b] $R^2 = 0.975$ for this fit.

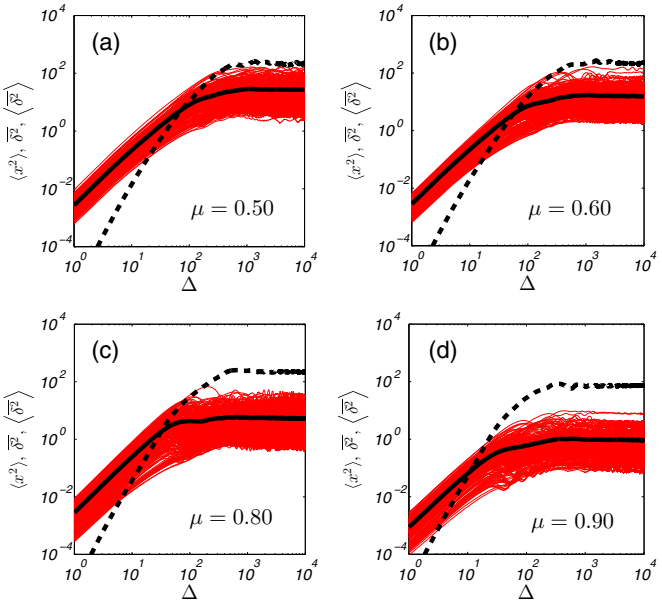

FIG. 6. The eMSD $\langle x^2(t)\rangle$ (thick dashed black curves, with $t \leftrightarrow \Delta$), tMSDs $\overline{\delta^2(\Delta)}$ (thin solid red/gray curves), and trajectory-averaged tMSD $\langle\overline{\delta^2(\Delta)}\rangle$ (thick solid black curves) for DBE transport with $\mu = 0.50$, 0.60, 0.80, and 0.90. All quantities are evaluated from $N = 256$ independent realizations ($T = 10^5$). Other parameters include $\sigma = 0.01$ and $\nu = 1$.

These simulation results further confirm the transient diffusion for short timescales. The inequivalence $\overline{\delta^2(\Delta)} \neq \langle x^2(\Delta)\rangle$ is valid for a certain parameter phase. On the other hand, with the power of DBE increasing, we find that, the eMSD and the trajectory-averaged tMSD seem to reach their plateau values at earlier times. A particular case is for $\mu = 0.90$, where the DBEs get localized after a much shorter diffusive process of ~200 TUs [as seen in Fig. 6(d)]. Such facts, in some degree, reflect the difference of the mobility between the low-power and the high-power DBEs.

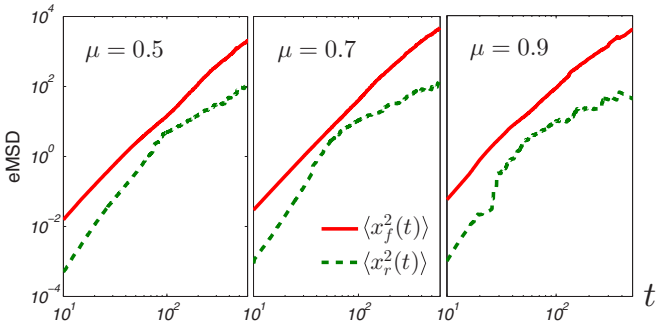

FIG. 7. Comparison of $\langle x_f^2(t)\rangle$ (solid red curves) and $\langle x_r^2(t)\rangle$ (dashed green curves) in the time interval $t \in [10, 600]$ for $\mu = 0.50$, 0.70, and 0.90. The parameters are $\sigma = 0.01$, $\nu = 1$, and $N = 256$. For most of the diffusive regimes, the value of $\langle x_f^2(t)\rangle$ is an order of magnitude larger than that of $\langle x_r^2(t)\rangle$.

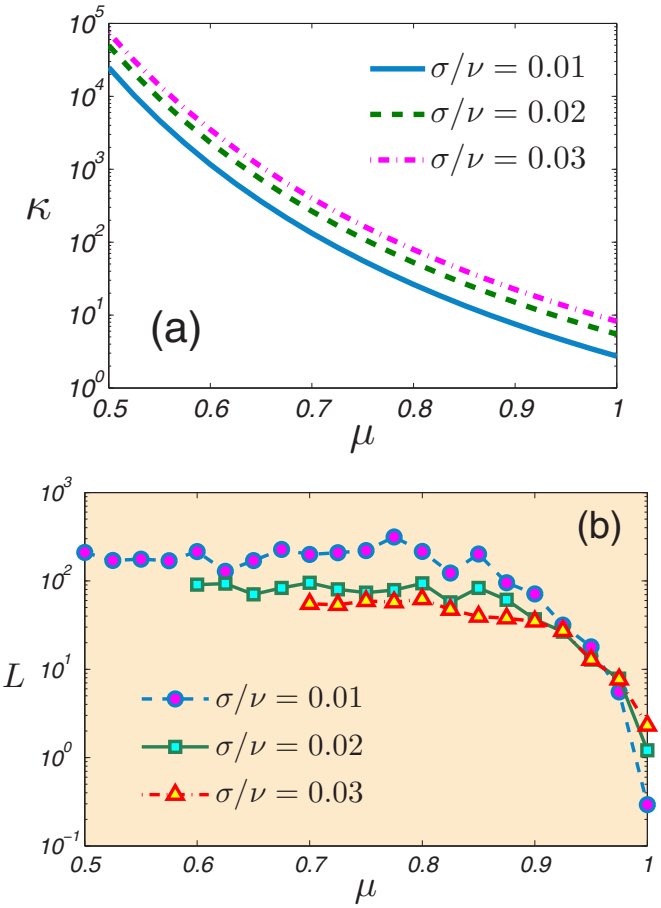

FIG. 8. (a) Plots of κ as functions of μ; (b) The dependence of L on μ. Other relevant parameters are $\nu = 1$ and $N = 256$.

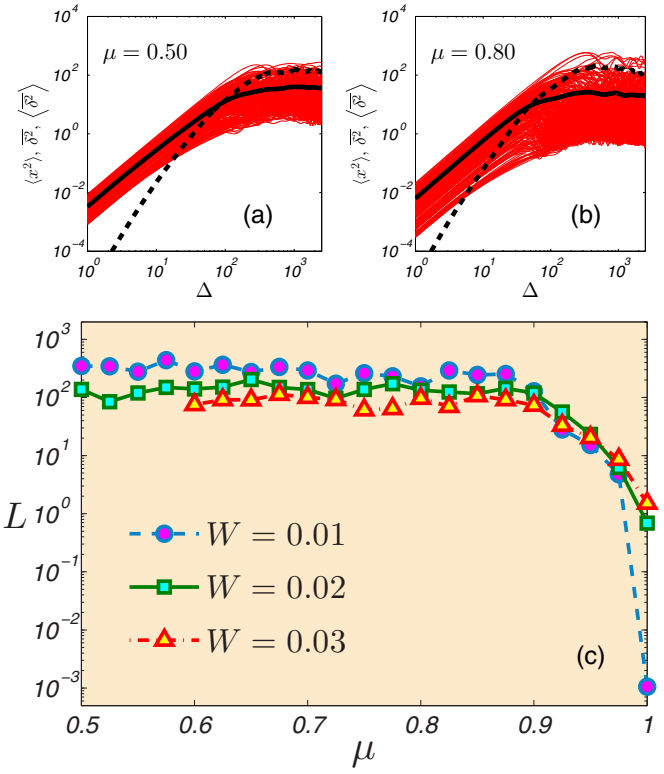

FIG. 9. The eMSD $\langle x^2(t)\rangle$ (thick dashed black curves, with $t \leftrightarrow \Delta$), tMSDs $\overline{\delta^2(\Delta)}$ (thin solid red/gray curves), and trajectory-averaged tMSD $\langle\delta^2(\Delta)\rangle$ (thick solid black curves) for the DBE transport with (a) $\mu = 0.50$; (b) $\mu = 0.80$ ($W = 0.02$ for both cases). (c) The dependence of L on μ. All quantities are evaluated from $N = 256$ independent realizations ($\nu = 1$).

APPENDIX C: ANALYSIS OF THE TRANSIENT DIFFUSION

As we divide the DBEs into two classes, the eMSD $\langle x^2(t)\rangle$ over N realizations can be separately expressed as

$$\begin{aligned}\langle x^2(t)\rangle &\equiv \frac{1}{N}\sum_{j=1}^{N} x_j^2(t)\\ &= \frac{1}{N}\left\{\sum_{k=1}^{N_f}\left[x_f^2(t)\right]_k + \sum_{l=1}^{N-N_f}\left[x_r^2(t)\right]_l\right\}\\ &= \frac{1}{N}\left[\langle x_f^2(t)\rangle N_f + \langle x_r^2(t)\rangle (N-N_f)\right]\\ &= \left[\langle x_f^2(t)\rangle - \langle x_r^2(t)\rangle\right]S(t) + \langle x_r^2(t)\rangle. \end{aligned} \tag{C1}$$

Note that $\langle x_f^2(t)\rangle$ and $\langle x_r^2(t)\rangle$ are respectively averaged over N_f and $N - N_f$ realizations. For a range of parameters ($\mu = 0.50$–0.90), numerical simulations generally reveal, as three examples shown in Fig. 7:

$$\langle x_f^2(t)\rangle \gg \langle x_r^2(t)\rangle. \tag{C2}$$

Thus, we derive the following approximation:

$$\langle x^2(t)\rangle \approx \langle x_f^2(t)\rangle S(t) + \langle x_r^2(t)\rangle. \tag{C3}$$

APPENDIX D: $\kappa(\mu)$ AND $L(\mu)$ FOR DIFFERENT σ

We consider the localization for stronger disorder ($\sigma = 0.02$ and $\sigma = 0.03$ are chosen, while $\nu = 1$ is set without loss of generality). The corresponding plots of κ, as functions of μ, are presented in Fig. 8(a). By extended simulations, the dependence of L on μ, for $\sigma = 0.02$ and $\sigma = 0.03$, is computed and compared with that for $\sigma = 0.01$, as seen in Fig. 8(b). Since a certain amount of low-power DBEs are likely to be destroyed by the stronger disorder, we record the values of L starting from $\mu = 0.60$ for $\sigma = 0.02$, and from $\mu = 0.70$ for $\sigma = 0.03$.

APPENDIX E: SELECTED SIMULATION RESULTS FOR $\epsilon_n \in$ unif$[-W, +W]$

We performed extended simulations for the uniformly distributed random potentials and found the DBE behaviors kept the similar features to those for the normally distributed random potentials. Two typical examples are presented in Figs. 9(a) and 9(b), demonstrating the transient diffusion with inequality between their eMSD and tMSD. Also, Fig. 9(c) shows the two-regime localization of DBEs for three different values of W.

[1] P. W. Anderson, Absence of diffusion in certain random lattices, Phys. Rev. **109**, 1492 (1958).

[2] M. Segev, Y. Silberberg, and D. N. Christodoulides, Anderson localization of light, Nat. Photon. **7**, 197 (2013).

[3] A. Mafi, Transverse Anderson localization of light: A tutorial, Adv. Opt. Photon. **7**, 459 (2015).

[4] S. Fishman, Y. Krivolapov, and A. Soffer, The nonlinear Schrödinger equation with a random potential: Results and puzzles, Nonlinearity **25**, R53 (2012).

[5] T. V. Laptyeva, M. V. Ivanchenko, and S. Flach, Nonlinear lattice waves in heterogeneous media, J. Phys. A **47**, 493001 (2014).

[6] K. Ø. Rasmussen, D. Cai, A. R. Bishop, and N. Grønbech-Jensen, Localization in a nonlinear disordered system, Europhys. Lett. **47**, 421 (1999).

[7] A. S. Pikovsky and D. L. Shepelyansky, Destruction of Anderson Localization by Weak Nonlinearity, Phys. Rev. Lett. **100**, 094101 (2008).

[8] S. Flach, D. O. Krimer, and C. Skokos, Universal Spreading of Wave Packets in Disordered Nonlinear Systems, Phys. Rev. Lett. **102**, 024101 (2009).

[9] T. Schwartz, G. Bartal, S. Fishman, and M. Segev, Transport and Anderson localization in disordered two-dimensional photonic lattices, Nature (London) **446**, 52 (2007).

[10] Y. Lahini, A. Avidan, F. Pozzi, M. Sorel, R. Morandotti, D. N. Christodoulides, and Y. Silberberg, Anderson Localization and Nonlinearity in One-Dimensional Disordered Photonic Lattices, Phys. Rev. Lett. **100**, 013906 (2008).

[11] C. Fort, L. Fallani, V. Guarrera, J. E. Lye, M. Modugno, D. S. Wiersma, and M. Inguscio, Effect of Optical Disorder and Single Defects on the Expansion of a Bose-Einstein Condensate in a One-Dimensional Waveguide, Phys. Rev. Lett. **95**, 170410 (2005).

[12] D. Clément, A. F. Varón, M. Hugbart, J. A. Retter, P. Bouyer, L. Sanchez-Palencia, D. M. Gangardt, G. V. Shlyapnikov, and A. Aspect, Suppression of Transport of an Interacting Elongated Bose-Einstein Condensate in a Random Potential, Phys. Rev. Lett. **95**, 170409 (2005).

[13] E. Kim, A. J. Martínez, S. E. Phenisee, P. G. Kevrekidis, M. A. Porter, and J. Yang, Direct measurement of superdiffusive energy transport in disordered granular chains, Nat. Commun. **9**, 640 (2018).

[14] D. K. Campbell, S. Flach, and Y. S. Kivshar, Localizing energy through nonlinearity and discreteness, Phys. Today **57**(1), 43 (2004).

[15] S. Flach and A. V. Gorbach, Discrete breathers-advances in theory and applications, Phys. Rep. **467**, 1 (2008).

[16] S. Aubry, Discrete breathers: Localization and transfer of energy in discrete Hamiltonian nonlinear systems, Physica D **216**, 1 (2006).

[17] R. Franzosi, R. Livi, G. L. Oppo, and A. Politi, Discrete breathers in Bose-Einstein condensates, Nonlinearity **24**, R89 (2011).

[18] B. Rumpf, Intermittent movement of localized excitations of a nonlinear lattice, Phys. Rev. E **70**, 016609 (2004).

[19] B. Rumpf, Transition behavior of the discrete nonlinear Schrödinger equation, Phys. Rev. E **77**, 036606 (2008).

[20] H. Hennig, T. Neff, and R. Fleischmann, Dynamical phase diagram of Gaussian wave packets in optical lattices, Phys. Rev. E **93**, 032219 (2016).

[21] H. Hennig, J. Dorignac, and D. K. Campbell, Transfer of Bose-Einstein condensates through discrete breathers in an optical lattice, Phys. Rev. A **82**, 053604 (2010).

[22] X. D. Bai, B. A. Malomed, and F. G. Deng, Unidirectional transport of wave packets through tilted discrete breathers in nonlinear lattices with asymmetric defects, Phys. Rev. E **94**, 032216 (2016).

[23] V. A. Brazhnyi, C. P. Jisha, and A. S. Rodrigues, Interaction of discrete nonlinear Schrödinger solitons with a linear lattice impurity, Phys. Rev. A **87**, 013609 (2013).

[24] J. P. Gordon and H. A. Haus, Random walk of coherently amplified solitons in optical fiber transmission, Opt. Lett. **11**, 665 (1986).

[25] V. Folli and C. Conti, Frustrated Brownian Motion of Nonlocal Solitary Waves, Phys. Rev. Lett. **104**, 193901 (2010).

[26] Z.-Y. Sun and X. Yu, Transport of nonautonomous solitons in two-dimensional disordered media, Ann. Phys. (Berlin) **529**, 1600323 (2017).

[27] Y. V. Kartashov, V. A. Vysloukh, and L. Torner, Brownian soliton motion, Phys. Rev. A **77**, 051802(R) (2008).

[28] L. M. Aycock, H. M. Hurst, D. K. Efimkin, D. Genkina, H.-I. Lu, V. M. Galitski, and I. B. Spielman, Brownian motion of solitons in a Bose-Einstein condensate, Proc. Natl. Acad. Sci. USA **114**, 2503 (2017).

[29] Y. V. Kartashov and V. A. Vysloukh, Anderson localization of solitons in optical lattices with random frequency modulation, Phys. Rev. E **72**, 026606 (2005).

[30] K. Sacha, C. A. Müller, D. Delande, and J. Zakrzewski, Anderson Localization of Solitons, Phys. Rev. Lett. **103**, 210402 (2009).

[31] M. Mochol, M. Płodzień, and K. Sacha, Dark soliton in a disorder potential, Phys. Rev. A **85**, 023627 (2012).

[32] Note that we also have used some numerically iterated stationary soliton solutions of Eq. (1) (without randomness) as the initial conditions and found the main features with respect to the transport are not changed.

[33] K. Ø. Rasmussen, T. Cretegny, P. G. Kevrekidis, and N. Grønbech-Jensen, Statistical Mechanics of a Discrete Nonlinear System, Phys. Rev. Lett. **84**, 3740 (2000).

[34] S. Iubini, L. Chirondojan, G.-L. Oppo, A. Politi, and P. Politi, Dynamical Freezing of Relaxation to Equilibrium, Phys. Rev. Lett. **122**, 084102 (2019).

[35] R. Metzler, J.-H. Jeon, A. G. Cherstvy, and E. Barkai, Anomalous diffusion models and their properties: non-stationarity, non-ergodicity, and ageing at the centenary of single particle tracking, Phys. Chem. Chem. Phys. **16**, 24128 (2014).

[36] I. Golding and E. C. Cox, Physical Nature of Bacterial Cytoplasm, Phys. Rev. Lett. **96**, 098102 (2006).

[37] J. Jeon, N. Leijnse, L. B. Oddershede, and R. Metzler, Anomalous diffusion and power-law relaxation of the time averaged mean squared displacement in worm-like micellar solutions, New J. Phys. **15**, 045011 (2013).

[38] N. Gal and D. Weihs, Experimental evidence of strong anomalous diffusion in living cells, Phys. Rev. E **81**, 020903(R) (2010).

[39] Y. Peng, L. Lai, Y.-S. Tai, K. Zhang, X. Xu, and X. Cheng, Diffusion of Ellipsoids in Bacterial Suspensions, Phys. Rev. Lett. **116**, 068303 (2016).

[40] P. Barthelemy, J. Bertolotti, and D. S. Wiersma, A Lévy flight for light, Nature (London) **453**, 495 (2008).

[41] I. Bronstein, Y. Israel, E. Kepten, S. Mai, Y. Shav-Tal, E. Barkai, and Y. Garini, Transient Anomalous Diffusion of Telomeres in the Nucleus of Mammalian Cells, Phys. Rev. Lett. **103**, 018102 (2009).

[42] For reliability of our numerics, we varied the step size by orders of magnitude ($\Delta t = 0.05$–0.001), and also altered the lattice size ($L = 200$–500), we found the results did not change. We even used a different integration scheme, the second-order Besse method [43,44], and the DBE behaviors had no significant changes either. For the Runge-Kutta scheme with $\Delta t = 0.01$, the relative errors of the conserved mass and energy for each integration step were usually kept smaller than 10^{-9} and 10^{-8} respectively.

[43] C. Besse, A relaxation scheme for the nonlinear Schrödinger equation, SIAM J. Numer. Anal. **42**, 934 (2004).

[44] X. Antoine, W. Bao, and C. Besse, Computational methods for the dynamics of the nonlinear Schrödinger/Gross-Pitaevskii equations, Comput. Phys. Commun. **184**, 2621 (2013).

[45] We checked the wave function $\psi_n(t)$ as an expansion in terms of the eigenstates and eigenvalues of the linear system ($\nu = 0$ and $\epsilon_n \neq 0$), and found the expansion coefficients presenting strong time-dependent oscillation, even for our final computational domain (e.g., the time interval $\Delta t = 1000$ before $t = 10^5$). This further reveals the contribution of nonlinearity to the evolution of wave packets up to $t = 10^5$.

[46] Y. He, S. Burov, R. Metzler, and E. Barkai, Random Time-Scale Invariant Diffusion and Transport Coefficients, Phys. Rev. Lett. **101**, 058101 (2008).

[47] Y. Meroz, I. M. Sokolov, and J. Klafter, Subdiffusion of mixed origins: When ergodicity and nonergodicity coexist, Phys. Rev. E **81**, 010101(R) (2010).

[48] A. Godec and R. Metzler, Finite-Time Effects and Ultraweak Ergodicity Breaking in Superdiffusive Dynamics, Phys. Rev. Lett. **110**, 020603 (2013).

[49] T. Mithun, Y. Kati, C. Danieli, and S. Flach, Weakly Nonergodic Dynamics in the Gross-Pitaevskii Lattice, Phys. Rev. Lett. **120**, 184101 (2018).

[50] Z.-Y. Sun, S. Fishman, and A. Soffer, Soliton mobility in disordered lattices, Phys. Rev. E **92**, 040903(R) (2015).

[51] G. Kopidakis, S. Komineas, S. Flach, and S. Aubry, Absence of Wave Packet Diffusion in Disordered Nonlinear Systems, Phys. Rev. Lett. **100**, 084103 (2008).

[52] Ch. Skokos, D. O. Krimer, S. Komineas, and S. Flach, Delocalization of wave packets in disordered nonlinear chains, Phys. Rev. E **79**, 056211 (2009).